

# Transformations between 2MASS, SDSS and BVRI photometric systems: bridging the near infrared and optical

S. Bilir,<sup>1\*</sup> S. Ak<sup>1</sup>, S. Karaali<sup>2</sup>, A. Cabrera-Lavers<sup>3,4</sup>, T. S. Chonis<sup>5</sup>, C. M. Gaskell<sup>5,6</sup>

<sup>1</sup>*Istanbul University Science Faculty, Department of Astronomy and Space Sciences, 34119, University-Istanbul, Turkey*

<sup>2</sup>*Beykent University, Faculty of Science and Letters, Department of Mathematics and Computer, Beykent 34398, Istanbul, Turkey*

<sup>3</sup>*Instituto de Astrofísica de Canarias, E-38205 La Laguna, Tenerife, Spain*

<sup>4</sup>*GTC Project Office, E-38205 La Laguna, Tenerife, Spain*

<sup>5</sup>*Department of Physics & Astronomy, University of Nebraska, Lincoln, NE 68588-0111, USA*

<sup>6</sup>*Present Address: Department of Astronomy, University of Texas, Austin, TX 78712-0259, USA*

Accepted 2007 month day. Received year month day;

## ABSTRACT

We present colour transformations for the conversion of the *2MASS* photometric system to the Johnson-Cousins *UBVRI* system and further into the *SDSS ugriz* system. We have taken *SDSS gri* magnitudes of stars measured with the 2.5-m telescope from *SDSS* Data Release 5 (DR5), and *BVRI* and *JHK<sub>s</sub>* magnitudes from Stetson’s catalogue and Cutri et al. (2003), respectively. We matched thousands of stars in the three photometric systems by their coordinates and obtained a homogeneous sample of 825 stars by the following constraints, which are not used in previous transformations: 1) the data are de-reddened, 2) giants are omitted, and 3) the sample stars selected are of the highest quality. We give metallicity, population type, and transformations dependent on two colours. The transformations provide absolute magnitude and distance determinations which can be used in space density evaluations at short distances where some or all of the *SDSS ugriz* magnitudes are saturated. The combination of these densities with those evaluated at larger distances using *SDSS ugriz* photometry will supply accurate Galactic model parameters, particularly the local space densities for each population.

**Key words:** surveys–catalogues–techniques: photometric

## 1 INTRODUCTION

Among several large surveys, two have been most widely used in recent years. The first, the Sloan Digital Sky Survey (*SDSS*; York et al. 2000), is the largest photometric and spectroscopic survey in optical wavelengths. Secondly, the Two Micron All Sky Survey (*2MASS*; Skrutskie et al. 2006) has imaged the sky across infrared wavelengths.

*SDSS* obtains images almost simultaneously in five broad bands (*u*, *g*, *r*, *i*, and *z*) centered at 3540, 4760, 6280, 7690 and 9250 Å, respectively (Fukugita et al. 1996; Gunn et al. 1998; Hogg et al. 2001; Smith et al. 2002). The photometric pipeline (Lupton et al. 2001) detects the objects, matches the data from the five filters, and measures instrumental fluxes, positions and shape parameters. The shape parameters allow the classification of objects as “point

source” (compatible with the point-spread function) or “extended”. The magnitudes derived from fitting a point-spread function (PSF) are currently accurate to about 2 per cent in *g*, *r*, and *i*, and 3–5 per cent in *u* and *z* for bright (< 20 mag) point sources. Data Release 5 (DR5) is almost 95 per cent complete for point sources to (*u*, *g*, *r*, *i*, *z*)=(22, 22.2, 22.2, 21.3, 20.5). The median full-width at half-maximum of the PSFs is about 1.5 arcsec (Abazajian et al. 2004). The data are saturated at about 14 mag in *g*, *r*, and *i*, and about 12 mag in *u* and *z* (see, for example, Chonis & Gaskell 2007).

*2MASS* provides the most complete database of near infrared (NIR) Galactic point sources available to date. During the development of this survey, two highly automated 1.3-m telescopes were used: one at Mt. Hopkins, Arizona to observe the Northern Sky, and the other at Cerro Tololo Observatory in Chile to complete the survey’s Southern half. Observations cover 99.998 per cent (Skrutskie et al. 2006) of the sky with simultaneous detections in *J* (1.25 μm), *H* (1.65 μm), and *K<sub>s</sub>* (2.17 μm) bands up to limiting mag-

\* E-mail: sbilir@istanbul.edu.tr

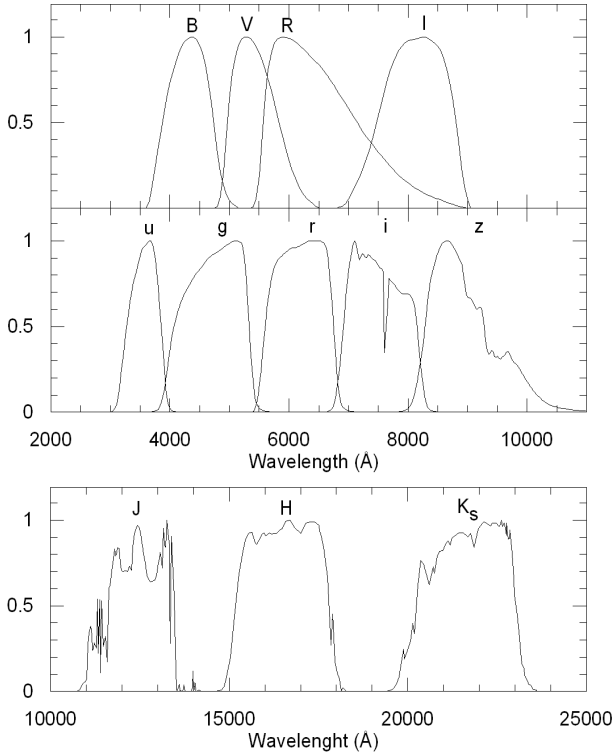


**Figure 1.** Normalized passbands of the Johnson-Cousins *BVRI* filters (upper panel), the *SDSS ugriz* filters (middle panel), and the *2MASS* filters (lower panel).

nititudes of 15.8, 15.1, and 14.3, respectively. Bright source extractions have  $1\sigma$  photometric uncertainty of  $< 0.03$  mag and astrometric accuracy on the order of 100 mas. Calibration offsets between any two points in the sky are  $< 0.02$  mag. The passband profiles for *BVRI*, *ugriz*, and *JHK<sub>s</sub>* photometric systems are given in Fig. 1.

It is important to derive transformations between a newly defined photometric system and those that are more traditional (such as the Johnson-Cousins *UBVRI* system). A number of transformations between *u'g'r'i'z'*, *ugriz* and *UBVR<sub>CIC</sub>* exist. The *u'g'r'i'z'* system is referred to the similar filter system used on the 0.5-m Photometric Calibration Telescope at *SDSS*. It should be noted that there are differences between the *u'g'r'i'z'* and *ugriz* systems. These are discussed in Tucker et al. (2006), Davenport et al. (2007), and Smith et al. (2007). In this paper we are concerned with transformation to and from the *ugriz* system of the 2.5-m. The first transformations derived between the *SDSS u'g'r'i'z'* system and the Johnson-Cousins photometric system were based on observations in *u'*, *g'*, *r'*, *i'*, and *z'* filters (Smith et al. 2002). In their work, the standards refer to the *SDSS* filter-detector combination used at the 1.0-m telescope at the US Naval Observatory. There are slight zero-point differences between these and the filters used at the 2.5-m telescope at Apache Point Observatory (APO) which lead to systematic differences between the magnitudes evaluated at the two observatories (Rider et al. 2004).

An improved set of transformations between the observations obtained in *u'g'r'* filters at the Isaac Newton Telescope (INT) at La Palma, Spain, and the Landolt's (1992) *UBV* standards is derived by Karaali, Bilir & Tunçel (2005).

The INT filters were designed to reproduce the *SDSS* system. Karaali et al. (2005) presented for the first time transformation equations depending on two colours.

Rodgers et al. (2006) considered two-colour or quadratic forms in their transformation equations. Jordi, Grebel & Ammon (2006) used *SDSS* DR4 and *BVRI* photometry taken from different sources and derived population (and metallicity) dependent transformation equations between *SDSS* and *UBVRI* systems. They also give transformation equations between the *SDSS* and *RGU* systems. *RGU* is a photographic system founded by Becker (1938), and used in the Basle Halo Program (Becker 1965) which presented the largest systematic survey of the Galaxy. The most recent work is by Chonis & Gaskell (2007) who used transformations from *SDSS ugriz* to *UBVRI* not depending on luminosity class or metallicity to determine CCD zero points.

The first transformations between *2MASS* and other photometric systems are those of Walkowicz, Hawley & West (2004) and West, Walkowicz & Hawley (2005) who determined the level of magnetic activity in M and L dwarfs. The aim of Davenport et al. (2006) in deriving equations between *2MASS* and other systems was to estimate the absolute magnitudes of cool stars. Covey et al. (2007) consider the *ugrizJHK* stellar locus (i.e., the position of main-sequence stars in the 7-dimensional colour diagram) and show how it can be used to identify objects with unusual colours. Our aim in the present paper is to derive transformation equations between *2MASS*, *SDSS* and *BVRI* which can be used for various applications. Our hope is that such equations may help Galactic researchers combine *2MASS* and *SDSS* data in model parameter estimations. Thus, *2MASS* data would be used to fill the space density gap at short distances where *SDSS* data are saturated. We will use all the procedures described in recent works which improve the transformations between pairs of systems to derive the most accurate transformation equations between the three photometric systems previously mentioned. Our transformation equations will be based on the currently available data (DR5; Adelman-McCarthy et al. 2007), and they will be dependent on luminosity, metallicity and two colours.

In Section 2 we present the sources of our star sample and the criteria applied to the chosen stars. The transformation equations are given in Section 3. Finally, in Section 4, we discuss our results.

## 2 DATA

The data used for our transformations were taken from sources previously discussed. The first main source of our data was the Stetson Catalogue. Stetson used a large set of multi-epoch CCD observations centered on Landolt fields and other regions in the sky and reduced them in a homogeneous manner tied to the Landolt *UBVRI* standards. The larger area coverage and greater sensitivity of the CCD observations compared to the earlier photomultiplier observations permitted Stetson to include stars down to  $V \sim 20$  mag. Since 2000, Stetson has been publishing a gradually growing list of suitable faint stars (Stetson 2000) with repeat

observations which can be found at the website of the Canadian Astronomy Data Center<sup>1</sup>. The Stetson catalogue contains only stars that were observed at least five times under photometric conditions with the standard error of the mean magnitude less than 0.02 mag in at least two of the four filters. Stetson’s database also contains fields not covered by Landolt (e.g., fields in globular clusters and in nearby resolved dwarf galaxies). While Landolt’s original fields contained mainly Population I stars, Stetson’s new fields also include a sizable fraction of Population II stars. Since Stetson’s catalogue does not include *U*-band photometry, we derive transformations for *BVRI* only. The available form of the catalogue has 40,090 stars.

The second source we use is *SDSS* DR5<sup>2</sup>. We selected the relevant standard star sample by matching Stetson’s published photometry to *SDSS* DR5 photometry. Matching of the stars was done with Robert Lupton’s SQL code which is published on the *SDSS* DR5 website. We obtained 3,798 stars by matching Stetson stars and *SDSS* DR5 stars.

The last source for our work is the *2MASS All-Sky Catalog of Point Sources* (Cutri et al. 2003). *2MASS* is not as deep of a survey as *SDSS*. Thus, only 1,984 out of the 3,798 stars overlapped with the Stetson data and the *SDSS* DR5 data. *2MASS* magnitudes are adopted from SIMBAD<sup>3</sup>.

The near infrared magnitudes of the 1,984 stars found in all three photometric systems are not as sensitive as their optical magnitudes. To select the more sensitive near infrared magnitudes of the selected stars, we used the magnitude flags, labelled “AAA”, which indicates the quality of the magnitudes for the three filters in the *2MASS* All-Sky Catalog of Point Sources (Cutri et al. 2003). After applying this selection criterion based on the quality of the data, the total number of sufficient stars in all three photometric systems was reduced to 886.

## 2.1 Reddening

The standard stars lie in fields with different Galactic latitudes, thus, each field has a different amount of reddening. Some stars in the sample are within 150 pc and therefore should not be affected by reddening from Galactic dust. The  $E(B - V)$  colour excesses of stars have been evaluated in two steps. First, we used the maps of Schlegel, Finkbeiner & Davis (1998) and evaluated an  $E_\infty(B - V)$  excess for each star. We then reduced them by the following procedure (Bahcall & Soneira 1980):

$$A_d(b) = A_\infty(b) \left[ 1 - \exp\left(\frac{-|d \sin(b)|}{H}\right) \right]. \quad (1)$$

Here,  $b$  and  $d$  are the Galactic latitude and distance of the star, respectively.  $H$  is the scaleheight for the interstellar dust which is adopted as 125 pc (Marshall et al. 2006) and  $A_\infty(b)$  and  $A_d(b)$  are the total absorptions for the model and for the distance to the star, respectively.  $A_\infty(b)$  can be evaluated by means of Eq. (2):

<sup>1</sup> <http://www2.cadc-ccda.hia-ihp.nrc-cnrc.gc.ca/community/STETSON/archive/>

<sup>2</sup> <http://www.sdss.org/dr5/>

<sup>3</sup> <http://simbad.u-strasbg.fr/simbad/>

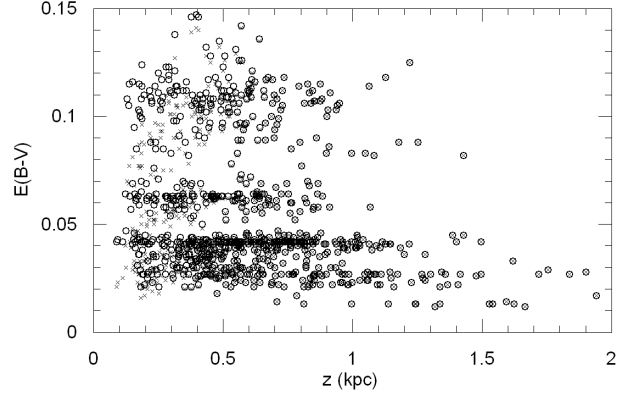


**Figure 2.**  $E(B - V)$  colour-excess versus height from the Galactic plane,  $z$ . The symbol (o) indicates the colour excess estimated by the procedure of Schlegel et al. (1998). (x) corresponds to the reduced colour excess (Bahcall & Soneira 1980).

$$A_\infty(b) = 3.1E_\infty(B - V). \quad (2)$$

$E_\infty(B - V)$  is the colour excess for the model taken from the NASA Extragalactic Database<sup>4</sup>. Then,  $E_d(B - V)$ , i.e. the colour excess for the corresponding star at the distance  $d$ , can be evaluated by Eq. (3) adopted for distance  $d$ ,

$$E_d(B - V) = A_d(b) / 3.1. \quad (3)$$

We have omitted the suffixes  $\infty$  and  $d$  from the colour excess  $E(B - V)$  in our tables and figures. However, we use the terms “model” for the colour excess of Schlegel et al. (1998) and “reduced” for the colour excess corresponding to distance  $d$ . The total absorption  $A_d$  used in this section and the classical total absorption  $A_V$  have the same meaning. As shown in Fig. 2, there are no differences between the model  $E(B - V)$  colour excesses and the reduced ones for heights larger than  $z \sim 0.5$  kpc above the Galactic plane. Here,  $z = d \sin(b)$ , where the distance  $d$  is evaluated by the combination of the apparent  $g$  and absolute  $M_g$  magnitudes of a star, i.e.  $g - M_g = 5 \log d - 5 + A_g$ , where  $A_g$  is the total absorption. The absolute magnitude of stars with  $4 < M_g \leq 8$  were determined by the procedure of Karaali et al. (2005), whereas for  $M_g > 8$ , we followed the procedure of Bilir, Karaali & Tunçel (2005).

In order to determine total absorptions,  $A_m$ , for the *SDSS* bands, we used  $A_m/A_v$  data given by Fan (1999), i.e. 1.593, 1.199, 0.858, and 0.639 for  $m=u, g, r,$  and  $i$ , respectively.

We used the equation of Cardelli, Clayton & Mathis (1989) for de-reddening the  $R - I$  colour and those of Fiorucci & Munari (2003) (see also; Bilir, Güver & Aslan 2006; Ak et al. 2007) for the *2MASS* magnitudes:

$$E(R - I) = 0.60E(B - V), \quad (4)$$

$$A_J = 0.887E(B - V), \quad (5)$$

$$A_H = 0.565E(B - V), \quad (6)$$

$$A_{K_s} = 0.382E(B - V). \quad (7)$$

All the colours and magnitudes with subscript “0” will be mentioned as de-reddened ones, hereafter.

<sup>4</sup> <http://nedwww.ipac.caltech.edu/forms/calculator.html>

**Table 1.** Johnson-Cousins, *SDSS*, and *2MASS* magnitudes of the sample stars (825 total stars). The columns give: (1) Star name; (2) and (3) Galactic coordinates; (4)  $V$ -apparent magnitude; (5) and (6)  $(B - V)$  and  $(R - I)$  colour indices; (7)  $g$ -apparent magnitude; (8), (9), and (10)  $(u - g)$ ,  $(g - r)$ ,  $(r - i)$  colour indices; (11)  $J$ -apparent magnitude; (12) and (13)  $(J - H)$ ,  $(H - K_s)$  colour indices, and (14) reduced  $E_d(B - V)$  colour excess. The complete table is available in electronic format.

(1) Star	(2) $l$ ( $^\circ$ )	(3) $b$ ( $^\circ$ )	(4) $V$	(5) $(B - V)$	(6) $(R - I)$	(7) $g$	(8) $(u - g)$	(9) $(g - r)$	(10) $(r - i)$	(11) $J$	(12) $(J - H)$	(13) $(H - K_s)$	(14) $E_d(B - V)$
L107-S61	5.437	41.308	18.472	1.499	1.054	19.334	2.695	1.466	0.796	15.357	0.775	-0.100	0.093
L107-S83	5.454	41.266	17.421	1.548	1.259	18.272	2.736	1.468	1.015	13.862	0.672	0.262	0.076
L107-S97	5.499	41.257	16.145	0.692	0.461	16.446	1.267	0.507	0.176	14.783	0.397	-0.081	0.103
...	...	...	...	...	...	...	...	...	...	...	...	...	...

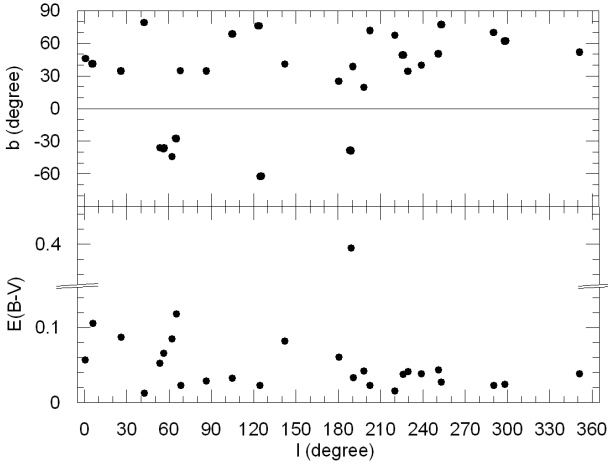


**Figure 3.** Galactic coordinates of the Stetson fields and the corresponding  $E(B - V)$  colour-excess of Schlegel et al. (1998).

The Galactic coordinates of the Stetson fields and the corresponding  $E(B - V)$  colour-excesses are given in Fig. 3. The field with  $E(B - V) > 0.4$  is omitted.

## 2.2 Separation of dwarfs and giants

The  $(u - g)_0 - (g - r)_0$  two-colour diagram (Fig. 4) of stars common in all three catalogues and with the best quality  $J$ ,  $H$ , and  $K_s$  magnitudes indicate that additional constraints are necessary to obtain a homogeneous star sample. There is an unexpected scattering and the stellar locus is wide. We adopted red stars (16 in total), with  $(u - g)_0 > 2.85$  mag which lie below the concentrated stellar locus as giants. Additionally, we identified 11 metal rich giants by the procedure of Ivezić et al. (2007) and omitted them from the sample. These authors calibrated the  $(u - g)_0 - (g - r)_0$  two-colour diagram with metallicity ( $[M/H]$ ) and surface gravity ( $\log g$ ) which provides dwarf-giant separation. The 11 stars mentioned above lie at the left of the locus with  $\log g = 2$  and  $[M/H] = 0$  dex, based on the Kurucz's (1979) stellar model. Finally, we used the following procedure of Helmi et al. (2003), and identified 33 stars as metal poor giants: This procedure is based on the Spaghetti Photometric Survey (SPS) (Morrison et al. 2000) with Washington photometry where metal poor stars could be isolated on the basis of (M-T2) and (M-51) colours, sensitive to temperature and strength of the Mg $b$  and Mg $H$  features near 5200Å,

respectively; and a first estimate of their luminosity classes were obtained. The candidates were observed spectroscopically and were classified into dwarfs and giants using the following indicators (Morrison et al. 2003): 1) The Mg $b$  and Mg $H$  features near 5200Å, which are characteristic of dwarfs and are almost absent in giant stars for  $0.8 \leq (B - V) \leq 1.3$ . 2) The CaI 4227Å line, which is usually present in dwarfs and absent in giants; may be visible in metal-poor giants with  $[M/H] < -1.5$ , and it is more conspicuous than the dwarfs of the same colour. 3) The CaII H and K lines near 3950Å, which are sensitive to  $[M/H]$ .

The  $(g - r)_0$  versus  $(u - g)_0$  colour-colour diagram of Helmi et al. (2003) for 19,000 stars brighter than  $r_0 = 19$  and whose photometric errors in all bands are less than 0.05 show a clear offset for nine *SPS* giants. The authors used the well-defined stellar locus to derive a principal axes coordinate system ( $P_1$ ,  $P_2$ ), where  $P_1$  lies parallel to the stellar locus and  $P_2$  measures the distance from it. The origin is chosen to coincide with the highest stellar density ( $(u - g)_0 = 1.21$ ,  $(g - r)_0 = 0.42$ ). Since the objects of interest occur in a relatively narrow colour range, they restricted their work to  $1.1 \leq (u - g)_0 \leq 2$  and  $0.3 \leq (g - r)_0 \leq 0.8$ . This procedure yields

$$\begin{aligned}
 P_1 &= 0.910(u - g)_0 + 0.415(g - r)_0 - 1.28, \\
 P_2 &= -0.415(u - g)_0 + 0.910(g - r)_0 + 0.12,
 \end{aligned}
 \tag{8}$$

The position of the locus in the  $r$  versus  $P_2$  colour-magnitude diagram depends on the  $r$  magnitudes, i.e. the median  $P_2$  colour becomes redder at the faint end. Helmi et al. (2003) corrected for this effect using a linear  $P_2$  versus  $r$  fit (the corrections varies from -0.03 to 0.05 mag). Thus, they defined the colour  $s$  that is normalized such that its error is approximately equal to the mean photometric error in a single band. They obtained

$$s = -0.249u_0 + 0.794g_0 - 0.555r_0 + 0.240.
 \tag{9}$$

The diagram  $r$  versus  $s$  show a symmetrical distribution for the star sample in question and a clear offset for the giants.

Based on the  $s$  colour distribution of the *SPS* giants and the overall  $s$  colour distribution, Helmi et al. (2003) selected metal-poor giants as stars with  $r_0 < 19$ ,  $-0.1 < P_1 < 0.6$  for  $1.1 \leq (u - g)_0 \leq 2$  and  $0.3 \leq (g - r)_0 \leq 0.8$ , and  $|s| > m_s + 0.05$ , where  $m_s$  is the median value of  $s$  in appropriately chosen subsamples.

Thus, the 60 total giants were excluded from the sample.

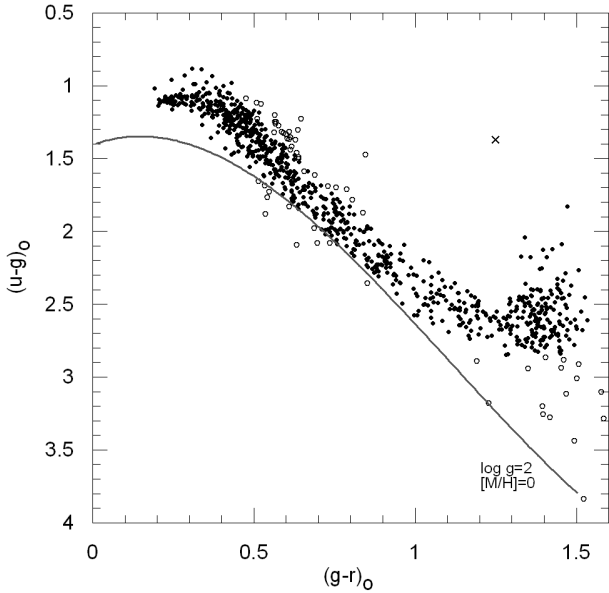


**Figure 4.** The position of giants (o) and dwarfs (●) in the  $(u - g)_0 - (g - r)_0$  two colour diagram, identified by the procedures of Ivezić et al. (2007) and Helmi et al. (2003). The cross (×) corresponds to the unidentified star. The solid line is based on the Kurucz's (1979) stellar model for  $\log g = 2$  and  $[M/H] = 0$  dex.

**Table 2.** Mean errors and standard deviations for the filters of Johnson-Cousins, *SDSS*, and *2MASS* photometries.

Filter	Mean error	$s$	Photometry
B	0.006	$\pm 0.005$	<i>BVRI</i>
V	0.004	0.003	
R	0.005	0.005	
I	0.004	0.004	
g	0.016	0.005	<i>SDSS</i>
r	0.015	0.005	
i	0.015	0.004	
J	0.036	0.011	<i>2MASS</i>
H	0.044	0.016	
$K_s$	0.058	0.024	

### 2.3 Final sample

We omitted one final standard from the sample due to its position in the two-colour diagrams (Fig. 4). The final sample includes 825 stars. Their *2MASS*  $JHK_s$ , *SDSS*  $gri$  and *BVRI* data are given Table 1. Also, the  $(u - g)_0 - (g - r)_0$  and  $(g - r)_0 - (r - i)_0$  two-colour diagrams are plotted in Fig. 5. The errors for the magnitudes in  $B$ ,  $V$ ,  $R$ ,  $I$ ,  $g$ ,  $r$ ,  $i$ ,  $J$ ,  $H$ , and  $K_s$  are presented in Table 2 and Fig. 6. The colour intervals covered by the standards are  $0.30 < (B - V)_0 < 1.70$ ,  $0.23 < (R - I)_0 < 1.78$ ,  $0.18 < (g - r)_0 < 1.54$ ,  $0 < (r - i)_0 < 1.65$ ,  $0 < (J - H)_0 < 0.98$ , and  $-0.23 < (H - K_s)_0 < 0.63$ .

The  $g_0$  histogram presented in Fig. 7 shows that our sample includes stars of different apparent magnitudes in a large range:  $14 < g_0 < 20$ . On the other hand, the  $(g - r)_0$  colour histogram in the same figure indicates a multi-modal distribution. This is very important because if the star sample consists of a combination of different population types and metallicities, then different transformation equations

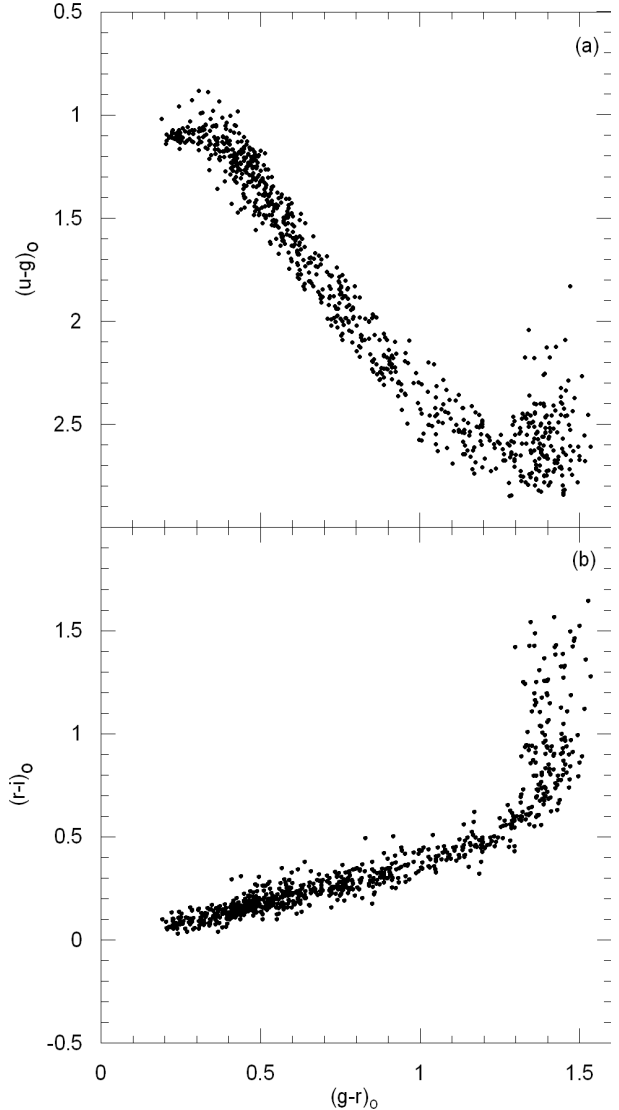


**Figure 5.** Two-colour diagrams of the sample (825 dwarfs). (a) the  $(u - g)_0 - (g - r)_0$  and (b) the  $(g - r)_0 - (r - i)_0$  diagram.

should be derived. We evaluated the metallicity of stars by the procedure given in Karaali et al. (2003). This procedure, defined for stars with  $0.10 < (g - r)_0 \leq 0.95$ , provides metallicities in the interval  $-2.7 \leq [M/H] \leq +0.1$  dex and is based on the calibration of the metallicity determined spectroscopically, where  $\delta_{0.43}$  is the ultraviolet excess of a star relative to a Hyades star of the same  $(g - r)_0$ , reduced to the colour  $(g - r)_0 = 0.43$  which corresponds to  $(B - V)_0 = 0.60$  in the *UBV*-system:  $[M/H] = 0.10 - 3.54\delta_{0.43} - 39.63\delta_{0.43}^2 + 63.51\delta_{0.43}^3$ . The restriction of  $(g - r)_0$  is due to the colour range of the sample used for the calibration. Red stars,  $(g - r)_0 > 0.95$ , are old thin disc dwarfs with a mean metallicity  $[M/H] = -0.1 \pm 0.3$  dex (Cox 2000). Hence we adopted the metallicity range for these stars as  $[M/H] > -0.4$  dex. We assumed stars with  $(g - r)_0 > 0.95$  to be metal-rich (Table 3). Fig. 8 shows that our sample covers stars with metallicities down to  $[M/H] = -3$  dex. The number of metal-poor stars ( $[M/H] \leq -1.2$  dex) is not negligible. Therefore, we separated the sample of stars into three metallicity categories: metal-rich stars ( $[M/H] > -0.4$  dex),

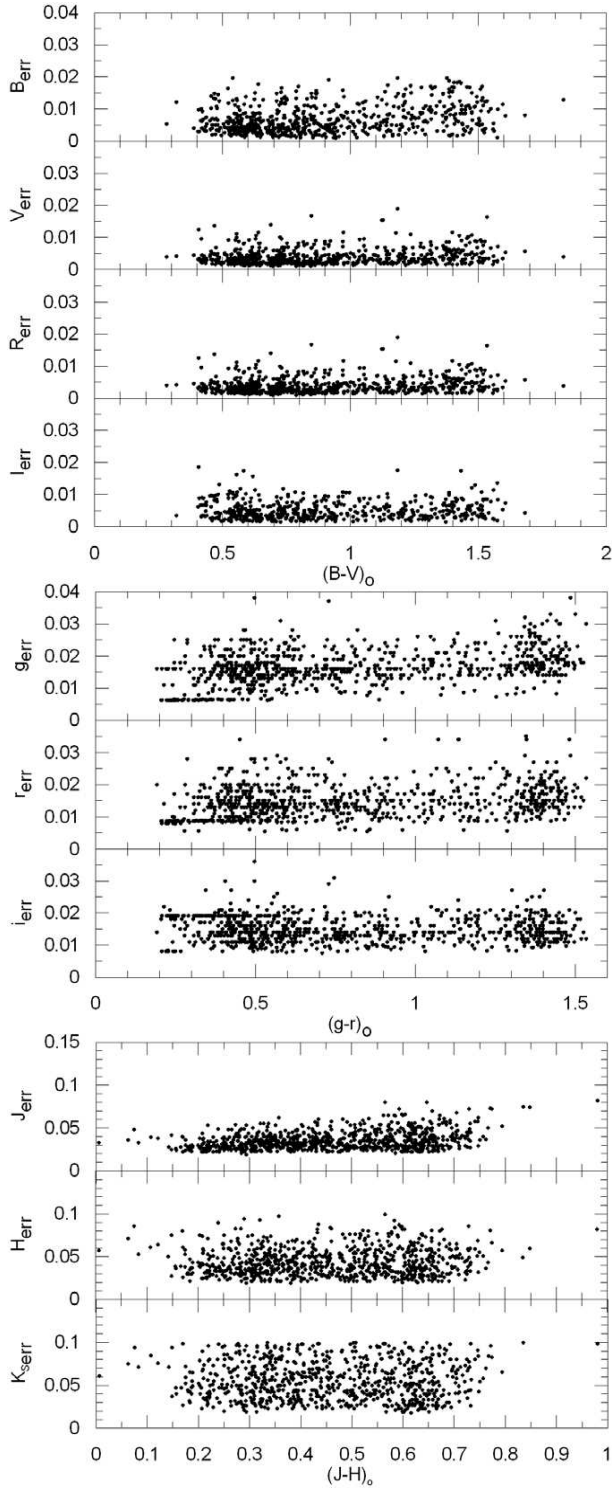


**Figure 6.** The error distributions for Johnson-Cousins  $BVRI$ ,  $SDSS\ gri$ , and  $2MASS\ JHK_s$ .

intermediate-metallicity stars ( $-1.2 < [M/H] \leq -0.4$  dex), and metal-poor stars ( $-3 < [M/H] \leq -1.2$  dex). Transformation equations for each set are evaluated.

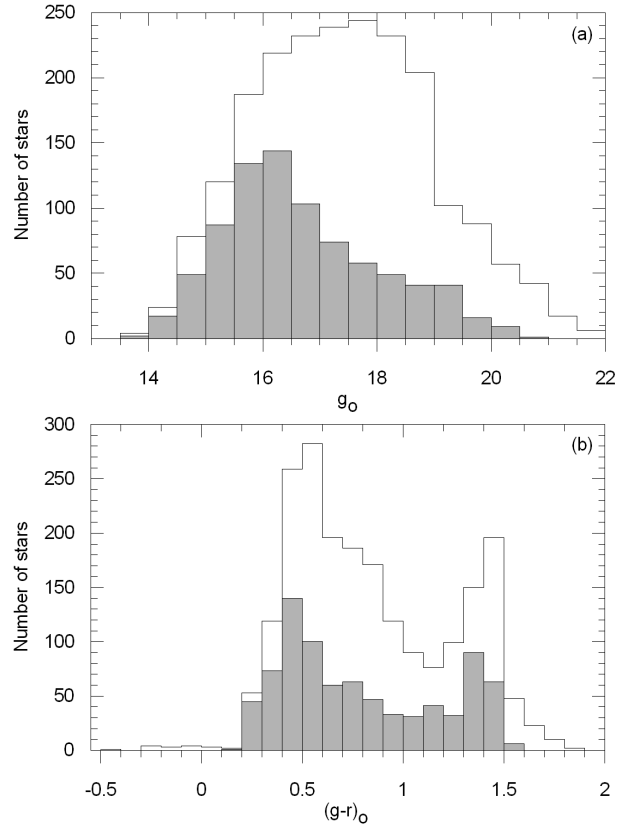


**Figure 7.** (a)  $g_0$  apparent magnitude histogram, and (b)  $(g-r)_0$  colour histogram for the “AAA” star sample (black area) and for the stars found in all three photometries (white area).

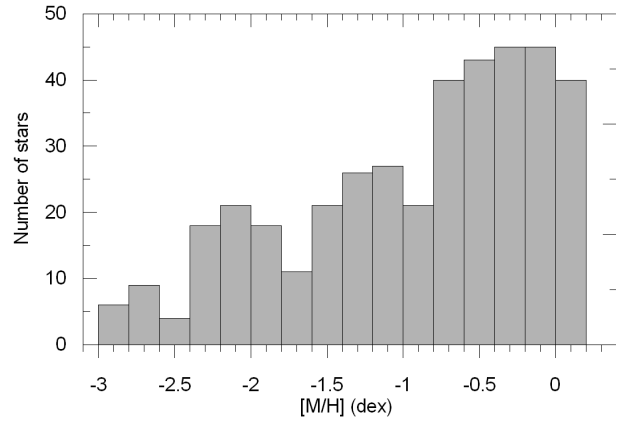


**Figure 8.** Metallicity distribution of the sample.

**Table 3.** Metallicity distribution of the sample. Stars with  $(g-r)_0 > 0.95$  mag were assumed to have a metallicity of  $-0.4 < [M/H]$  dex.

Metallicity (dex)	Number of stars
$-0.4 < [M/H]$	505
$-1.2 < [M/H] \leq -0.4$	131
$-3.0 < [M/H] \leq -1.2$	189

### 3 RESULTS

#### 3.1 Transformations between *2MASS* and Johnson-Cousins photometry

We used the following general equations and derived four sets of transformations between *2MASS* and Johnson-Cousins *BVRI*. The sets of transformations consist of: 1) transformations for the whole sample (825 stars), 2) transformations for metal-rich stars, 3) transformations for intermediate metallicity stars, and 4) transformations for metal-poor stars. The definition of the last three sub-samples are already given in the previous section. The general equations are:

$$(V - J)_0 = a_1(B - V)_0 + b_1(R - I)_0 + c_1, \quad (10)$$

$$(V - H)_0 = a_2(B - V)_0 + b_2(R - I)_0 + c_2, \quad (11)$$

$$(V - K_s)_0 = a_3(B - V)_0 + b_3(R - I)_0 + c_3. \quad (12)$$

The numerical values of the coefficients  $a_i$ ,  $b_i$  and  $c_i$  ( $i=1, 2, 3$ ) for the four sets are given in Table 4. The fourth and fifth numbers in each column are the squared correlation coefficient and the standard deviation for the colour indicated at the top of the column. There are differences between the values of the coefficients evaluated for the largest sample (825 stars) and the three sub samples. However, the coefficients for metal-rich stars are close to those corresponding to the total sample. The same similarity can be seen for the intermediate metallicity stars and the metal-poor stars. The metallicity distribution of these sub samples ( $-0.4 < [M/H]$ ,  $-1.2 < [M/H] \leq -0.4$ , and  $-3 < [M/H] \leq -1.2$  dex) remind us of the metallicity ranges depending on stellar location in thin or thick discs or the halo, respectively. That is, the transformations are luminosity and metallicity dependent. On the other hand, the coefficients  $a_i$  and  $b_i$  for the same equation are numerically comparable, suggesting that the transformations are two-colour dependent. Thus, if we derived transformations depending on a single colour, accuracy would be lost. In some works (cf., Jordi et al. 2006, for example) transformations were dependent on a single colour and the authors compensate by using a step function.

#### 3.2 Transformations between *2MASS* and *SDSS*

The transformations between *2MASS* and *SDSS* have similar general equations, given below:

$$(g - J)_0 = d_1(g - r)_0 + e_1(r - i)_0 + f_1, \quad (13)$$

$$(g - H)_0 = d_2(g - r)_0 + e_2(r - i)_0 + f_2, \quad (14)$$

$$(g - K_s)_0 = d_3(g - r)_0 + e_3(r - i)_0 + f_3. \quad (15)$$

The numerical values of the coefficients  $d_i$ ,  $e_i$  and  $f_i$  ( $i = 1, 2, 3$ ) for the four sets defined above, are given in Table 5. The transformations between *2MASS* and *SDSS* are also luminosity, metallicity, and two-colour dependent for the same reasons explained in Section 3.1.

#### 3.3 Residuals

We compared the observed colours and those evaluated via Eqs. (10) – (15). The mean of the residuals are smaller than

a thousandth. These residuals can be found in Table 6. The standard deviations, also given in Table 6, are close to 0.1 for all colours. The residuals are plotted versus observed  $(B - V)_0$  or  $(g - r)_0$  colours in Fig. 9. Although the number of stars are not equal in each bin, there is no systematic deviation from the zero point in any panel. However, the ranges of the residuals for different colours are not the same. Those resulting from Eqs. (10) and (13) are the smallest. The ranges of the residuals are larger for the longer-wavelength magnitudes. That is, for the  $J$  magnitude, the residual  $\Delta(V - J)$  and  $\Delta(g - J)$  lies between  $-0.2$  and  $+0.2$ , with a few exceptions, whereas  $\Delta(V - H)$ ,  $\Delta(g - H)$ ,  $\Delta(V - K_s)$  and  $\Delta(g - K_s)$  extend down to  $-0.4$  and up to  $+0.4$ . This indicates that the  $J$  (absolute) magnitudes evaluated via the transformations given above would be more accurate.

We did not show the plots of actual transformations. However, the comparison of the residuals, for the entire sample, for two-colours and one-colour transformations in Fig. 10 show that our transformations are much better than those for the one-colour ones. The scatter for one-colour transformations is much larger than that for two-colours and additionally there is a systematic deviation the one-colour transformations.

#### 3.4 Inverse transformation formulae

One may need to transform *2MASS* data to Johnson-Cousins system or *SDSS* system. Hence, we derived the inverse transformation formulae of Eqs. (10)–(12) and (13)–(15) as follows. We reduced the Eqs. (10)–(12) to two equations by eliminating the  $V$  magnitude. The solution of these equations gives the Johnson-Cousins colours  $(B - V)_0$  and  $(R - I)_0$  as a function of  $(J - H)_0$  and  $(H - K_s)_0$ . The general equations are:

$$(B - V)_0 = \alpha_1(J - H)_0 + \beta_1(H - K_s)_0 + \gamma_1, \quad (16)$$

$$(R - I)_0 = \alpha_2(J - H)_0 + \beta_2(H - K_s)_0 + \gamma_2. \quad (17)$$

We derived the following general equations for the *SDSS* colours, i.e.  $(g - r)_0$  and  $(r - i)_0$ , by applying the same procedure to the Eqs. (13)–(15).

$$(g - r)_0 = \alpha_3(J - H)_0 + \beta_3(H - K_s)_0 + \gamma_3, \quad (18)$$

$$(r - i)_0 = \alpha_4(J - H)_0 + \beta_4(H - K_s)_0 + \gamma_4. \quad (19)$$

The numerical values of the coefficients  $\alpha_i$ ,  $\beta_i$ , and  $\gamma_i$  ( $i=1, 2, 3, 4$ ) for the four sets mentioned above are given in Table 7.

### 4 CONCLUSION

We have presented the colour transformations for the conversion of the *2MASS* photometric system into the Johnson-Cousins *BVRI* system and further into the *SDSS gri* system. We have added some constraints to the dataset in addition to those of other authors who derived transformations between *SDSS ugriz* and other systems in order to obtain the most accurate transformations possible. The overall constraints used were as follows: 1) the data were de-reddened, 2) giants have been identified and excluded from the sample, 3) sample stars have been selected by the quality of the data, 4) transformations have been derived for sub-samples

**Table 4.** Coefficients  $a_i$ ,  $b_i$ , and  $c_i$  for the transformation equations (10), (11), and (12), in column matrix form for the four star categories. The subscript  $i=1, 2$ , and  $3$  correspond to the same number that denotes the columns. Numerical values in the fourth and fifth lines of each category are the squared correlation coefficients ( $R^2$ ) and the standard deviations ( $s$ ), respectively.

		(1)	(2)	(3)
Category		$(V - J)_o$	$(V - H)_o$	$(V - K_s)_o$
Total sample	$a_i$	$1.210 \pm 0.032$	$1.816 \pm 0.039$	$1.896 \pm 0.044$
	$b_i$	$1.295 \pm 0.038$	$1.035 \pm 0.046$	$1.131 \pm 0.052$
	$c_i$	$-0.046 \pm 0.014$	$0.016 \pm 0.017$	$-0.004 \pm 0.019$
	$R^2$	0.983	0.982	0.980
	$s$	0.098	0.119	0.133
$-0.4 < [M/H]$	$a_i$	$1.180 \pm 0.042$	$1.815 \pm 0.050$	$1.878 \pm 0.058$
	$b_i$	$1.346 \pm 0.045$	$1.062 \pm 0.052$	$1.165 \pm 0.061$
	$c_i$	$-0.051 \pm 0.023$	$-0.015 \pm 0.027$	$-0.018 \pm 0.032$
	$R^2$	0.985	0.984	0.981
	$s$	0.103	0.121	0.142
$-1.2 < [M/H] \leq -0.4$	$a_i$	$1.557 \pm 0.111$	$2.109 \pm 0.157$	$2.031 \pm 0.150$
	$b_i$	$0.461 \pm 0.205$	$0.612 \pm 0.290$	$0.878 \pm 0.277$
	$c_i$	$0.049 \pm 0.049$	$-0.016 \pm 0.069$	$0.004 \pm 0.066$
	$R^2$	0.902	0.894	0.906
	$s$	0.080	0.113	0.108
$-3.0 < [M/H] \leq -1.2$	$a_i$	$1.542 \pm 0.081$	$1.920 \pm 0.108$	$2.044 \pm 0.123$
	$b_i$	$0.447 \pm 0.156$	$0.845 \pm 0.207$	$0.974 \pm 0.237$
	$c_i$	$0.095 \pm 0.036$	$0.055 \pm 0.048$	$-0.022 \pm 0.054$
	$R^2$	0.943	0.942	0.936
	$s$	0.084	0.112	0.128

**Table 5.** Coefficients  $d_i$ ,  $e_i$ , and  $f_i$  for the transformation equations (13), (14), and (15), in column matrix form for the four star categories. The subscript  $i=1, 2$ , and  $3$  correspond to the same number that denotes the columns. Numerical values in the fourth and fifth lines of each category are the squared correlation coefficients ( $R^2$ ) and the standard deviations ( $s$ ), respectively.

		(1)	(2)	(3)
Category		$(g - J)_o$	$(g - H)_o$	$(g - K_s)_o$
Total sample	$d_i$	$1.379 \pm 0.015$	$1.849 \pm 0.021$	$1.907 \pm 0.023$
	$e_i$	$1.702 \pm 0.019$	$1.536 \pm 0.025$	$1.654 \pm 0.028$
	$f_i$	$0.518 \pm 0.007$	$0.666 \pm 0.010$	$0.684 \pm 0.011$
	$R^2$	0.994	0.991	0.990
	$s$	0.083	0.115	0.126
$-0.4 < [M/H]$	$d_i$	$1.361 \pm 0.016$	$1.823 \pm 0.022$	$1.881 \pm 0.024$
	$e_i$	$1.724 \pm 0.019$	$1.561 \pm 0.026$	$1.675 \pm 0.028$
	$f_i$	$0.521 \pm 0.009$	$0.670 \pm 0.013$	$0.692 \pm 0.014$
	$R^2$	0.995	0.993	0.992
	$s$	0.080	0.111	0.121
$-1.2 < [M/H] \leq -0.4$	$d_i$	$1.536 \pm 0.102$	$1.792 \pm 0.134$	$1.790 \pm 0.143$
	$e_i$	$1.400 \pm 0.215$	$2.092 \pm 0.281$	$2.272 \pm 0.301$
	$f_i$	$0.488 \pm 0.028$	$0.584 \pm 0.037$	$0.628 \pm 0.039$
	$R^2$	0.928	0.924	0.918
	$s$	0.085	0.112	0.120
$-3.0 < [M/H] \leq -1.2$	$d_i$	$1.435 \pm 0.061$	$1.711 \pm 0.075$	$1.741 \pm 0.086$
	$e_i$	$1.769 \pm 0.137$	$2.339 \pm 0.169$	$2.640 \pm 0.192$
	$f_i$	$0.481 \pm 0.022$	$0.598 \pm 0.027$	$0.583 \pm 0.031$
	$R^2$	0.960	0.960	0.954
	$s$	0.088	0.108	0.123



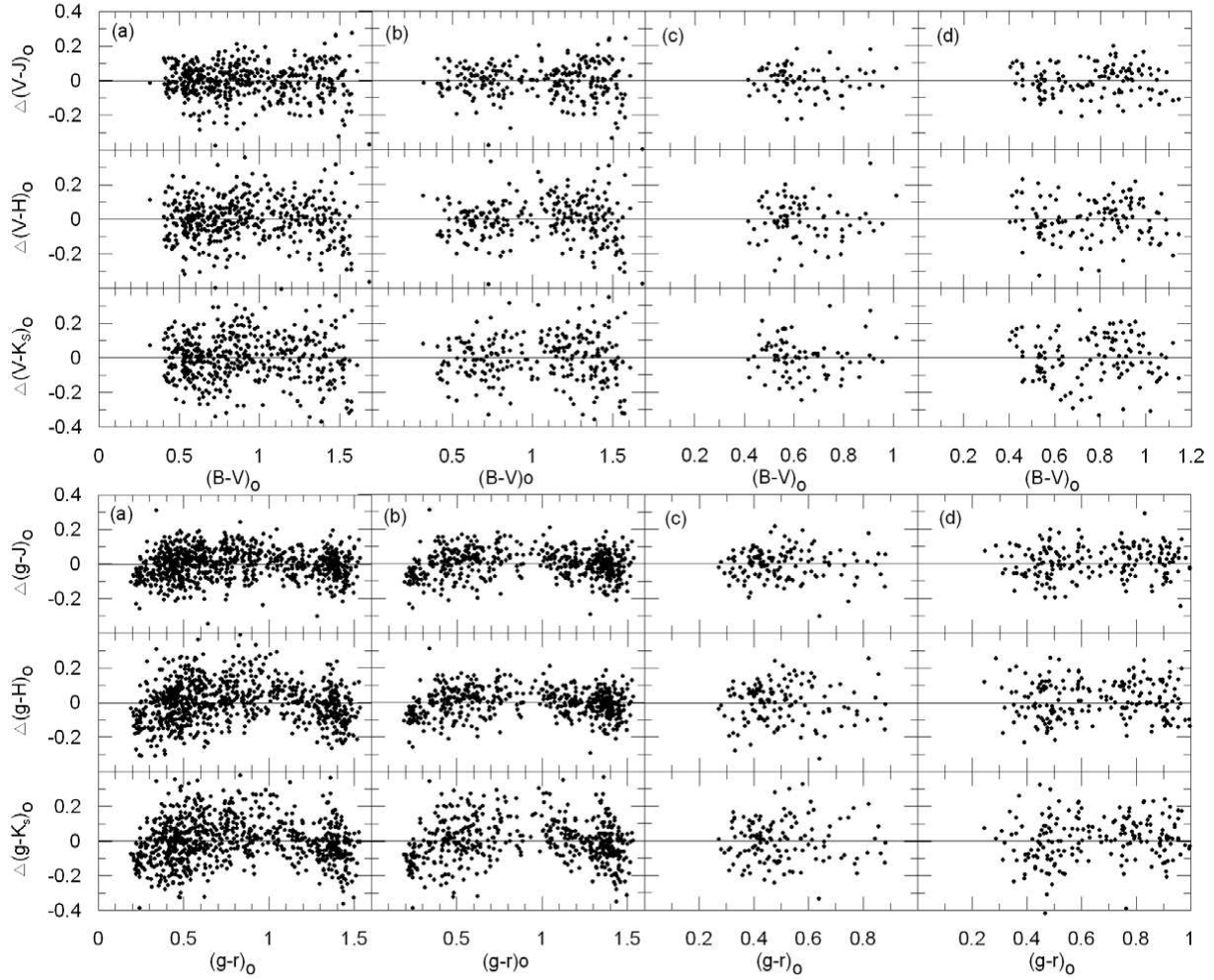


**Figure 9.** Colour residuals, for four star categories. The notation used is  $\Delta(\text{colour}) = (\text{evaluated colour}) - (\text{measured colour})$ . The four categories are (from left to right) (a) the entire sample, (b) high metallicity (metal-rich), (c) intermediate metallicity, and (d) low metallicity (metal-poor).

**Table 6.** Averages and standard deviations ( $s$ ) for differences between the measured and calculated colours (residuals) for six colours in all four star categories. The notation used is  $\Delta(\text{colour}) = (\text{evaluated colour}) - (\text{measured colour})$ .

Category		$\Delta(V - J)_o$	$\Delta(V - H)_o$	$\Delta(V - K_s)_o$	$\Delta(g - J)_o$	$\Delta(g - H)_o$	$\Delta(g - K_s)_o$
Total sample	average	-0.0002	-0.0004	0.0001	0.0008	0.0002	0.0006
	$s$	0.098	0.119	0.133	0.083	0.114	0.126
$-0.4 < [M/H]$	average	-0.0002	0.0000	-0.0001	-0.0002	-0.0004	-0.0007
	$s$	0.103	0.121	0.141	0.080	0.111	0.121
$-1.2 < [M/H] \leq -0.4$	average	0.0004	0.0001	-0.0004	0.0000	0.0003	0.0001
	$s$	0.079	0.112	0.107	0.085	0.111	0.119
$-3.0 < [M/H] \leq -1.2$	average	0.0001	0.0001	0.0000	-0.0003	-0.0004	0.0002
	$s$	0.084	0.111	0.127	0.087	0.107	0.122

of different metallicity and populations type, and 5) transformations are two colour dependent. The constraints described in items (1), (2), and (3) are new. Constraint (3) is especially important for 2MASS data because the inherent errors are larger relative to those in others photometries

The squared correlation coefficients ( $R^2$ ) for the transformations carried out for the four categories (i.e., the entire sample, the metal-rich stars, the intermediate metallicity stars, and the metal-poor stars) are rather high (see

Tables 4 and 5). The smallest of those is  $R^2 = 0.894$  for the colour  $(V - H)_o$ . All others lie between 0.900 and 0.995. The standard deviation is 0.1. The coefficients of the colour terms in the same transformation equation are compatible (see Table 4 and Table 5) which indicate that the transformations are two-colour dependent. On the other hand, there are differences between the corresponding transformation coefficients for the four categories. This is most conspicuous for metal-rich and metal-poor stars. That is, our

**Table 7.** Coefficients for the inverse transformation equations for four star categories.  $\alpha_i$ ,  $\beta_i$ , and  $\gamma_i$  ( $i = 1, 2, 3$  and  $4$ ) correspond to Eqs. (16), (17), (18) and (19), respectively. The numerical values of the coefficients are indicated on the same line of the corresponding star category.

Johnson-Cousins system						$(B - V)_0 = \alpha_1(J - H)_0 + \beta_1(H - K_s)_0 + \gamma_1$					$(R - I)_0 = \alpha_2(J - H)_0 + \beta_2(H - K_s)_0 + \gamma_2$				
Category	$\alpha_1$	$\beta_1$	$\gamma_1$	$R^2$	$s$	$\alpha_2$	$\beta_2$	$\gamma_2$	$R^2$	$s$					
Total Sample	1.622±0.032	0.912±0.051	0.044±0.015	0.845	0.120	0.954±0.028	0.593±0.050	0.025±0.013	0.755	0.101					
$-0.4 < [M/H]$	1.640±0.044	1.033±0.075	0.050±0.022	0.855	0.125	1.027±0.040	0.658±0.080	-0.003±0.020	0.772	0.117					
$-1.2 < [M/H] \leq -0.4$	1.103±0.074	0.486±0.091	0.228±0.029	0.665	0.077	0.521±0.054	0.311±0.066	0.179±0.021	0.546	0.050					
$-3.0 < [M/H] \leq -1.2$	1.276±0.056	0.541±0.066	0.173±0.025	0.782	0.088	0.608±0.038	0.322±0.051	0.172±0.017	0.712	0.054					
SDSS system						$(g - r)_0 = \alpha_3(J - H)_0 + \beta_3(H - K_s)_0 + \gamma_3$					$(r - i)_0 = \alpha_4(J - H)_0 + \beta_4(H - K_s)_0 + \gamma_4$				
Category	$\alpha_3$	$\beta_3$	$\gamma_3$	$R^2$	$s$	$\alpha_4$	$\beta_4$	$\gamma_4$	$R^2$	$s$					
Total Sample	1.951±0.032	1.199±0.050	-0.230±0.015	0.879	0.135	0.991±0.026	0.792±0.042	-0.210±0.012	0.760	0.107					
$-0.4 < [M/H]$	1.991±0.040	1.348±0.066	-0.247±0.019	0.900	0.136	1.000±0.036	1.004±0.064	-0.220±0.017	0.779	0.120					
$-1.2 < [M/H] \leq -0.4$	1.217±0.078	0.491±0.091	0.050±0.030	0.663	0.083	0.600±0.035	0.268±0.040	-0.049±0.013	0.708	0.037					
$-3.0 < [M/H] \leq -1.2$	1.422±0.065	0.600±0.076	-0.003±0.029	0.749	0.099	0.609±0.030	0.279±0.035	-0.047±0.013	0.728	0.045					

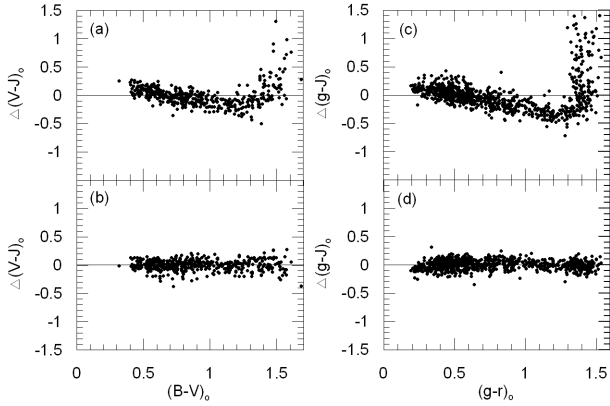


**Figure 10.**  $\Delta(V - J)_0$  and  $\Delta(g - J)_0$  colour residuals versus observed  $(B - V)_0$  or  $(g - r)_0$ , as an example. (a) and (c) for one-colour transformations, (b) and (d) for two-colour transformations.

transformations are metallicity dependent. Additionally, the metallicity ranges of the three sub samples,  $-0.4 < [M/H]$ ,  $-1.2 < [M/H] \leq -0.4$ , and  $-3 < [M/H] \leq -1.2$  dex, correspond to that for a thin disc, thick disc, and halo (i.e., the transformations are also luminosity dependent).

The mean of the residuals (i.e. the colour differences between those measured and those calculated) are less than  $\pm 0.001$  mag (see Table 6). The deviations of the measured colours from the calculated ones are small for  $(V - J)_0$ ,  $\pm 0.2$ , but relatively larger for redder colours ( $\pm 0.3$  for  $(V - H)_0$  and  $(V - K_s)_0$  for most of the stars (Fig. 9). Thus, the  $J$  absolute magnitudes will yield the best estimations. Davenport et al. (2006) did not give any residuals for  $\mathcal{Z}MASS$  data and thus we cannot compare their transformations with ours. However, the deviations of the measured colours from those calculated are not larger than those claimed by the authors cited above (cf. see Figures 4 and 6 of Jordi et al. 2006). If we take into account that the errors for  $\mathcal{Z}MASS$  data are larger than the errors of the photometries used in other recent transformations (such as between Johnson-Cousins  $UBVRI$  and  $SDSS$   $ugriz$  data), and that the data are non-simultaneous, we can say that our transformations are quite accurate.

## 5 ACKNOWLEDGMENTS

We would like to thank James Davenport, the referee, for his useful and constructive comments concerning the manuscript. This research used the facilities of the Canadian Astronomy Data Centre operated by the National Research Council of Canada with the support of the Canadian Space Agency.

Funding for the  $SDSS$  and  $SDSS-II$  has been provided by the Alfred P. Sloan Foundation, the Participating Institutions, the National Science Foundation, the U.S. Department of Energy, the National Aeronautics and Space Administration, the Japanese Monbukagakusho, the Max Planck Society, and the Higher Education Funding Council for England. The  $SDSS$  Web Site is <http://www.sdss.org/>.  $SDSS$  is managed by the Astrophysical Research Consortium for the participating institutions.

This publication makes use of data products from the Two Micron All Sky Survey, which is a joint project of the University of Massachusetts and the Infrared Processing and Analysis Center/California Institute of Technology, funded by the National Aeronautics and Space Administration and the National Science Foundation.

This research has made use of the SIMBAD, NASA's Astrophysics Data System Bibliographic Services and the NASA/IPAC Extragalactic Database (NED) which is operated by the Jet Propulsion Laboratory, California Institute of Technology, under contract with the National Aeronautics and Space Administration.

## REFERENCES

- Abazajian K., Adelman-McCarthy J. K., Agueros M. A., et al., 2004, *AJ*, 128, 502  
 Adelman-McCarthy J. K., et al., 2007, *VizieR On-line Data Catalog: II/276*  
 Ak T., Bilir S., Ak S., Retter A., 2007, *NewA*, 12, 446  
 Bahcall J. N., Soneira R. M., 1980, *ApJS*, 44, 73  
 Becker W., 1938, *Z. Astrophys*, 15, 225  
 Becker W., 1965, *Z. Astrophys*, 62, 54  
 Bilir S., Karaali S., Tunçel S., 2005, *AN*, 326, 321  
 Bilir S., Güver T., Aslan M., 2006, *AN*, 327, 693  
 Cardelli J. A., Clayton G. C., Mathis J. S., 1989, *ApJ*, 345, 245  
 Chonis T. S., Gaskell C. M., 2007, *AJ* (in press), (astro/ph:0710.5801)

- Covey K. R., et al., 2007, *AJ*, 134, 2398
- Cox A. N., 2000, *Allen's astrophysical quantities*, New York: AIP Press; Springer, Edited by Arthur N. Cox. ISBN: 0387987460
- Cutri R. M., et al., 2003, *2MASS All-Sky Catalog of Point Sources*, CDS/ADC Electronic Catalogues, 2246
- Davenport J. R. A., West A. A., Matthiesen C. K., Schmieding M., Kobelski A., 2006, *PASP*, 118, 1679
- Davenport J. R. A., Bochanski J. J., Covey K. R., Hawley S. L., West A. A., Schneider D. P., 2007, *AJ*, 134, 2430
- Fan X., 1999, *AJ*, 117, 2528
- Fiorucci M., Munari U., 2003, *A&A*, 401, 781
- Fukugita M., Ichikawa T., Gunn J. E., Doi M., Shimasaku K., Schneider D. P., 1996, *AJ*, 111, 1748
- Helmi A., Ivezić Z., Prada F., Pentericci L., Rockosi C. M., Schneider D. P., Grebel E. K., Harbeck D., Lupton R. H., Gunn J. E., Knapp G. R., Strauss M. A., Brinkmann J., 2003, *ApJ*, 586, 195
- Hogg D. W., Finkbeiner D. P., Schlegel D. J., Gunn J. E., 2001, *AJ*, 122, 2129
- Ivezić Z., Allyn Smith J., Miknaitis G., Lin H., Tucker D., et al., 2007, *AJ*, 134, 973
- Gunn J.E., Carr M., Rockosi C., et al., 1998, *AJ*, 116, 3040
- Jarrett T. H., Chester T., Cutri R., Schneider S., Skrutskie M., Huchra J. P., 2000, *AJ*, 119, 2498
- Jordi K., Grebel E. K., Ammon K., 2006, *A&A*, 460, 339
- Karaali S., Bilir S., Karataş Y., Ak S. G., 2003, *PASA*, 20, 165
- Karaali S., Bilir S., Tunçel S., 2005, *PASA*, 22, 24
- Kurucz R. L., 1979, *ApJS*, 40, 1
- Landolt A. U., 1992, *AJ*, 104, 340
- Lupton R. H., Gunn J. E., Ivezić Z., Knapp G. R., Kent S., Yasuda N., 2001, in *ASP Conf. Ser.: Astronomical Data Analysis Software and Systems X*, ed. F. R. Harden Jr., F. A. Primini and H. E. Payne, 238, 269
- Marshall D. J., Robin A. C., Reylé C., Schultheis M., Picaud S., 2006, *A&A*, 453, 635
- Morrison H. L., Mateo M., Olszewski E. W., Harding P., Dohm-Palmer R. C., Freeman K. C., Norris J. E., Morita M., 2000, *AJ*, 119, 2254
- Morrison H. L., Norris J., Mateo M., Harding P., Olszewski E. W., Shectman S. A., Dohm-Palmer R. C., Helmi A., Freeman K. C., 2003, *AJ*, 125, 2502
- Rider C. J., Tucker D. L., Smith J. A., Stoughton C., Allam S. S., Neilsen E. H., 2004, *AJ*, 127, 2210
- Rodgers C. T., Canterna R., Smith J. A., Pierce M. J., Tucker D. L., 2006, *AJ*, 132, 989
- Schlegel D. J., Finkbeiner D. P., Davis M., 1998, *ApJ*, 500, 525
- Skrutskie M. F., Cutri R. M., Stiening R., et al., 2006, *AJ*, 131, 1163
- Smith J. A., Tucker D. L., Kent S., Richmond M. W., Fukugita M., Ichikawa T., Ichikawa S., Jorgensen A. M., Uomoto A., Gunn J. E., 2002, *AJ*, 123, 2121
- Smith J. A., Tucker D. L., Allam S. S., Ivezić Z., Yanny B., Gunn J. E., Knapp G. R., Eisenstein D., Finkbeiner D., Fukugita M., 2007, *The Future of Photometric, Spectrophotometric and Polarimetric Standardization*, ASP Conference Series, Vol. 364, Edited by C. Sterken, San Francisco: Astronomical Society of the Pacific, p. 91
- Stetson P. B., 2000, *PASP*, 112, 925
- Tucker D. L., et al. 2006, *AN*, 327, 821
- Walkowicz L. M., Hawley S. L., West A. A., 2004, *PASP*, 116, 1105
- West A. A., Walkowicz L. M., Hawley S. L., 2005, *PASP*, 117, 706
- York D. G., et al., 2000, *AJ*, 120, 1579